Outage probability analysis of RIS-assisted RSMA systems over Nakagami-*m* fading channels

Nguyen Hong Kiem[1], Tran Manh Hoang[1*], Nguyen Tuan Minh[2], Le Thi Thanh Huyen[3]

[1]Telecommunications University, 101 Mai Xuan Thuong Street, Bac Nha Trang, Khanh Hoa, Vietnam;
[2]Institute of Information Technology and Electronics, Academy of Military Science and Technology, 17 Hoang Sam, Nghia Do, Hanoi, Vietnam;
[3]The Faculty of Radio Electronics Engineering, Le Quy Don Technical University, 236 Hoang Quoc Viet, Nghia Do, Hanoi, Vietnam.
[*]Corresponding author: tranmanhhoang@tcu.edu.vn
Received 5 Aug. 2025; Revised 23 Sep. 2025; Accepted 10 Oct. 2025; Published 30 Oct. 2025.
DOI: https://doi.org/10.54939/1859-1043.j.mst.IITE.2025.72-82

ABSTRACT

In this study, we propose and analyze an RIS-assisted rate-splitting multiple access (RSMA) system. The framework enhances transmission efficiency by simultaneously exploiting both the direct and RIS-reflected links to serve two users. For practical considerations, imperfect successive interference cancellation (SIC) is taken into account. Under the Nakagami-m fading channel model, closed-form expressions for the outage probability (OP) and energy efficiency (EE) are derived and verified through Monte Carlo simulations with a large number of iterations. Furthermore, a comprehensive comparative analysis with a benchmark RIS-assisted non-orthogonal multiple access (NOMA) scheme is conducted. Simulation results show that the proposed system significantly outperforms its NOMA counterpart in terms of OP. The impacts of key system parameters, including the number of RIS reflecting elements, transmit power, carrier frequency, fading severity, and SIC imperfection level, are thoroughly investigated. These findings demonstrate the strong potential of RIS-assisted RSMA as a promising solution to enhance the reliability of future sixth-generation (6G) wireless networks.

Keywords: Outage probability; Energy efficiency; Rate-splitting multiple access; Reconfigurable intelligent surface; Imperfect successive interference cancellation.

1. INTRODUCTION

Multiple access techniques play a fundamental role in simultaneously meeting the requirements of high data throughput, massive connectivity, and ultra-low latency, which are essential characteristics of industrial internet of things (IIoT), fifth generation (5G) networks, and future wireless communication systems [1]. In the evolution toward advanced wireless communications, technologies such as orthogonal frequency-division multiple access (OFDMA), non-orthogonal multiple access (NOMA), and massive multiple-input multiple-output (MIMO) have been developed to enhance spectral efficiency and improve overall network performance [2]. Among the advanced multiple access techniques, rate-splitting multiple access (RSMA) has emerged as an effective and adaptive solution, based on the strategy of dividing user messages into common and private parts. This approach enables more flexible decoding, allows efficient interference management, and helps maintain stable quality of service [3]. Thanks to these advantages, RSMA is particularly well-suited for heterogeneous and dynamic network environments such as IoT, 5G, and next-generation communication systems [4].

In addition to improving wireless system performance, one of the most promising enabling technologies for sixth-generation (6G) networks is the reconfigurable intelligent surface (RIS), which provides flexible control over the wireless propagation environment to boost both spectral and energy efficiency. In [5], the authors proposed a method to maximize the achievable data rate by employing passive intelligent mirrors, which are considered a precursor to modern RIS

technology. As a metasurface composed of numerous discrete and passive elements, RIS can dynamically adjust its reflection coefficients to manipulate the wireless environment. As a result, significant improvements in both spectral and energy efficiency can be achieved.

Motivated by the compelling advantages of RIS and RSMA, recent research has explored their joint integration to optimize wireless network performance. In particular, RIS-assisted RSMA-based wireless systems have emerged as a promising direction due to their potential to substantially improve key performance indicators, such as energy efficiency [6, 7] and spectral efficiency [8], [9]. In [10], RSMA is applied in a RIS-assisted cloud radio access network (C-RAN) to enhance the energy efficiency of the system. In [11], a two-layer RSMA-based multi-RIS system is proposed, where each RIS is strategically deployed at the cell edge to support edge users.

To the best of our knowledge, most existing studies on RIS-assisted RSMA systems are conducted under the assumption that the direct link between the transmitter and user equipments (UEs) is absent, i.e., signals are received exclusively via the RIS-reflected link, while the contribution of the direct link is largely neglected. To bridge this research gap, this paper proposes a two-user single-input single-output (SISO) transmission model in which each user simultaneously receives signals from both the direct and RIS-reflected links. This modeling approach not only offers a more realistic and comprehensive representation of the wireless propagation environment but also exploits the complementary advantages of both transmission paths to improve the overall system performance.

The main contributions of this paper are summarized as follows

• A novel two-user RSMA communication framework assisted by a RIS is proposed and analyzed under Nakagami-m fading channels, in which each user simultaneously receives signals from both the direct and RIS-reflected links. Closed-form expressions for the outage probability (OP) and energy efficiency (EE) of users D_1 and D_2 are derived based on signal-to-interference-plus-noise ratio (SINR) analysis and rigorously validated through Monte Carlo simulations.

• A systematic comparison between RIS-assisted RSMA and RIS-assisted NOMA systems is conducted, showing that the proposed scheme consistently outperforms in terms of OP and EE.

• The impact of key system parameters, including transmit power, number of RIS elements, power allocation factors, and the imperfection level of SIC, is investigated to evaluate the performance of individual users.

2. SYSTEM MODEL AND ANALYSIS

2.1. System and signal modeling

In this study, we consider an RIS-assisted RSMA network, where a source node (S) transmits messages to two RSMA users, denoted as D_k with $k \in \{1,2\}$, with the assistance of a reconfigurable intelligent surface (RIS) comprising a total of N elements, as shown in figure 1. Specifically, both users D_k simultaneously receive reflected signals from the RIS as well as direct signals transmitted by S. All wireless channels in the proposed system are assumed to follow the Nakagami-*m* fading. The channel coefficients of the links from S to the RIS, from the RIS to user D_k and directly from S to user D_k, are denoted as $\mathbf{h}_{\mathrm{SR}_i} \in \mathbb{C}^{N\times 1}$, $\mathbf{h}_{\mathrm{R}_i,\mathrm{D}_1} \in \mathbb{C}^{N\times 1}$, $\mathbf{h}_{\mathrm{R}_i,\mathrm{D}_2} \in \mathbb{C}^{N\times 1}$, and h_{SD_k}, respectively.

The S employed the RSMA technique to simultaneously transmit two messages, denoted as Ω_1 and Ω_2, intended for users D_1 and D_2, respectively. Each message Ω_n is partitioned into a common part Ω_{c_n} and a private part Ω_{p_n}, where $n = \{1,2\}$.

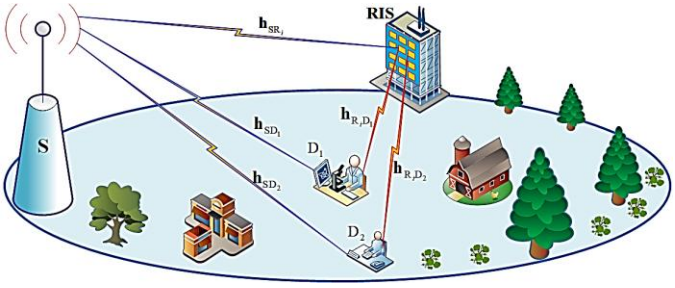

Figure 1. *RIS-assisted SISO system utilizes RSMA.*

The common parts Ω_{c_1} and Ω_{c_2}, intended for both users, are combined into a common stream s_c, which can be decoded by both users. In contrast, the private parts Ω_{p_1} and Ω_{p_2}, intended for individual users, are transmitted via two separate private streams, denoted as s_1 and s_2, respectively. The transmitted streams are organized into a vector $\mathbf{s}=\left[s_c, s_1, s_2\right]^T$. Consequently, the final transmit signal from S can be expressed as follows

$$x_{\mathrm{S}} = \sqrt{\beta_c P_{\mathrm{S}}} s_c + \sum_{k=1}^{2} \sqrt{\beta_k P_{\mathrm{S}}} s_k \tag{1}$$

where P_{S} is the transmit power of S, while β_c, β_1 and β_2 represent the power allocation coefficients for s_c and s_1, s_2, respectively, with $\beta_c + \beta_1 + \beta_2 = 1$. The received signal at D_k, ,comprising both direct and RIS reflected components, is given by

$$y_{\mathrm{D}_k} = \left(h_{\mathrm{SD}_k} + \sum_{i=1}^{N} h_{\mathrm{SR}_i} h_{\mathrm{R}_i\mathrm{D}_k} \right) x_{\mathrm{S}} + \eta_{\mathrm{D}_k} \tag{2}$$

where h_{SD_k}, h_{SR_i} and $h_{\mathrm{R}_i\mathrm{D}_k}$ are the channel coefficients from S to D_k, S to the i^{th} elements of the RIS, from the i^{th} elements of the RIS to D_k, respectively. Since the channel coefficients h_{SD_k}, h_{SR_i} and $h_{\mathrm{R}_i\mathrm{D}_k}$ are complex numbers, they can be represented through their magnitude and phase as follows: $h_{\mathrm{SD}_k} = a_{\mathrm{SD}_k} e^{-j\psi_{\mathrm{SD}_k}}$, $h_{\mathrm{SR}_i} = a_{\mathrm{SR}_i} e^{-j\psi_{\mathrm{SR}_i}}$ and $h_{\mathrm{R}_i\mathrm{D}_k} = a_{\mathrm{R}_i\mathrm{D}_k} e^{-j\psi_{\mathrm{R}_i\mathrm{D}_k}}$, where a_{SD_k}, a_{SR_i} and $a_{\mathrm{R}_i\mathrm{D}_k} \in (0,1]$ denote the magnitudes of h_{SD_k}, h_{SR_i} and $h_{\mathrm{R}_i\mathrm{D}_k}$, respectively. ψ_{SD_k}, ψ_{SR_i} and $\psi_{\mathrm{R}_i\mathrm{D}_k} \in (0, 2\pi]$ represents the phase angle. η_{D_k} is the additive white Gaussian noise (AWGN) at D_k with zero mean and variance of $\delta^2_{\mathrm{D}_k}$, i.e., $\eta_{\mathrm{D}_k} \sim \mathcal{CN}\left(0, \delta^2_{\mathrm{D}_k}\right)$, formula (2) can be rewritten as

$$\begin{aligned} y_{\mathrm{D}_k} &= \left(a_{\mathrm{SD}_k} e^{-j\psi_{\mathrm{SD}_k}} + \sum_{i=1}^{N} a_{\mathrm{SR}_i} a_{\mathrm{R}_i\mathrm{D}_k} e^{j(\psi_i - \psi_{\mathrm{SR}_i} - \psi_{\mathrm{R}_i\mathrm{D}_k})} \right) x_{\mathrm{S}} + \eta_{\mathrm{D}_k} \\ &= e^{-j\psi_{\mathrm{SD}_k}} \left(a_{\mathrm{SD}_k} + \sum_{i=1}^{N} a_{\mathrm{SR}_i} a_{\mathrm{R}_i\mathrm{D}_k} e^{j(\psi_i + \psi_{\mathrm{SD}_k} - \psi_{\mathrm{SR}_i} - \psi_{\mathrm{R}_i\mathrm{D}_k})} \right) x_{\mathrm{S}} + \eta_{\mathrm{D}_k} \end{aligned} \tag{3}$$

According to [12], the phase shifts are adjusted to maximize the SINR at D_k, where the optimal phase shift for the i^{th} RIS element is calculated as $\psi_i = \psi_{\mathrm{SR}_i} + \psi_{\mathrm{R}_i\mathrm{D}_k} - \psi_{\mathrm{SD}_k}$. After optimal phase alignment and setting $a_{\mathrm{SD}_k} + \sum_{i=1}^{N} a_{\mathrm{SR}_i} a_{\mathrm{R}_i\mathrm{D}_k} = \mathcal{X}$, expression (3) can be reformulated as

$$y_{\mathrm{D}_k} = e^{-j\psi_{\mathrm{SD}_k}} \mathcal{X} x_{\mathrm{S}} + \eta_{\mathrm{D}_k} \tag{4}$$

From (4), the SINR at the destination D_k can be given as

$$\gamma_c^{\mathrm{D}_k} = \frac{\left|e^{-j\psi_{\mathrm{SD}_k}}\right|^2 \mathcal{X}^2 P_{\mathrm{S}} \beta_c}{\left|e^{-j\psi_{\mathrm{SD}_k}}\right|^2 \mathcal{X}^2 P_{\mathrm{S}} (\beta_1 + \beta_2) + \delta_{\mathrm{D}_k}^2} \text{ and } \gamma_{p_k}^{\mathrm{D}_k} = \frac{\left|e^{-j\psi_{\mathrm{SD}_k}}\right|^2 \mathcal{X}^2 P_{\mathrm{S}} \beta_k}{\left|e^{-j\psi_{\mathrm{SD}_k}}\right|^2 \mathcal{X}^2 P_{\mathrm{S}} (\zeta\beta_c + \beta_{j=\{1,2\}, j\neq k}) + \delta_{\mathrm{D}_k}^2} \tag{5}$$

where $k=1$, $j=2$ or $k=2$, $j=1$, since $\left|e^{-j\psi_{\mathrm{SD}_k}}\right|^2 = 1$, from (5), the SINR is given by

$$\gamma_c^{\mathrm{D}_k} = \frac{\mathcal{X}^2 P_{\mathrm{S}} \beta_c}{\mathcal{X}^2 P_{\mathrm{S}} (\beta_1 + \beta_2) + \delta_{\mathrm{D}_k}^2} \text{ and } \gamma_{p_k}^{\mathrm{D}_k} = \frac{\mathcal{X}^2 P_{\mathrm{S}} \beta_k}{\mathcal{X}^2 P_{\mathrm{S}} (\zeta\beta_c + \beta_j) + \delta_{\mathrm{D}_k}^2} \tag{6}$$

Additionally, the study focuses on analyzing the outage probability of the proposed system over Nakagami-*m* fading channels. Accordingly, the statistical characteristics of the channel amplitude $\mathcal{X} \in \left\{a_{\mathrm{SD}_k}, a_{\mathrm{SR}_i}, a_{\mathrm{R}_i\mathrm{D}_k}\right\}$ are described by its cumulative distribution function (CDF) and probability density function (PDF), given below

$$F_{\mathcal{X}}(y) = \frac{1}{\Gamma(m_{\mathcal{X}})} \gamma(m_{\mathcal{X}}, \frac{m_{\mathcal{X}}}{\Omega_{\mathcal{X}}} y^2) = 1 - \frac{1}{\Gamma(m_h)} \gamma(m_h, \frac{m_h}{\Omega_h} y^2), \quad y \geq 0 \tag{7}$$

$$f_{\mathcal{X}}(y) = \frac{2 m_{\mathcal{X}}^{m_{\mathcal{X}}}}{\Gamma(m_{\mathcal{X}}) \Omega_{\mathcal{X}}^{m_{\mathcal{X}}}} y^{2m_{\mathcal{X}}-1} \exp(-\frac{m_{\mathcal{X}}}{\Omega_{\mathcal{X}}} y^2), \quad y \geq 0 \tag{8}$$

where, $\Omega_{\mathcal{X}}$ and $m_{\mathcal{X}}$ denote the spread and shape parameters, respectively.

2.2. Outage probability analysis

OP is particularly relevant in scenarios where maintaining reliable connectivity is essential, such as mission-critical communications, rural networks, and disaster recovery.

In the proposed RIS-assisted RSMA system, the OP at receiver D_k is defined as the event where D_k fails to successfully decode either the common stream s_c or its intended private stream s_1, s_2. Consequently, the OP at D_k can be formulated as

$$\begin{aligned} \mathrm{OP}_{\mathrm{out}}^{\mathrm{D}_k} &= \Pr\left\{\left(\gamma_c^{\mathrm{D}_k} < \gamma_{\mathrm{th}}^c\right) \cup \left(\gamma_{p_k}^{\mathrm{D}_k} < \gamma_{\mathrm{th}}^{p_k}\right)\right\} \\ &= \Pr\left\{\left(\frac{\mathcal{X}^2 P_{\mathrm{S}} \beta_c}{\mathcal{X}^2 P_{\mathrm{S}} (\beta_1 + \beta_2) + \delta_{\mathrm{D}_k}^2} < \gamma_{\mathrm{th}}^c\right) \cup \left(\frac{\mathcal{X}^2 P_{\mathrm{S}} \beta_k}{\mathcal{X}^2 P_{\mathrm{S}} (\zeta\beta_c + \beta_j) + \delta_{\mathrm{D}_k}^2} < \gamma_{\mathrm{th}}^{p_k}\right)\right\} \end{aligned} \tag{9}$$

$$\mathrm{OP}_{\mathrm{out}}^{\mathrm{D}_k} = \Pr\left\{\left(\mathcal{X}^2 P_{\mathrm{S}} (\beta_c - (\beta_1 + \beta_2)\gamma_{\mathrm{th}}^c) < \delta_{\mathrm{D}_k}^2 \gamma_{\mathrm{th}}^c\right) \cup \left(\mathcal{X}^2 P_{\mathrm{S}} (\beta_k - (\zeta\beta_c + \beta_j)\gamma_{\mathrm{th}}^{p_k}) < \delta_{\mathrm{D}_k}^2 \gamma_{\mathrm{th}}^{p_k}\right)\right\} \tag{10}$$

here, γ_{th}^c and $\gamma_{\mathrm{th}}^{p_k}$ denote the SINR thresholds for the common and private streams, respectively, with $\gamma_{\mathrm{th}}^c = 2^{R_c} - 1$, and $\gamma_{\mathrm{th}}^{p_k} = 2^{R_{p_k}} - 1$. These thresholds correspond to the target transmission rates R_c and R_{p_k} of the respective streams.

From equation (10), it can be observed that when $\beta_c - (\beta_1 + \beta_1)\gamma_{\mathrm{th}}^c \leq 0$ or $\beta_k - (\zeta\beta_c + \beta_j)\gamma_{\mathrm{th}}^{p_k} \leq 0$, (10) is always true. Therefore, $\mathrm{OP}_{\mathrm{out}}^{\mathrm{D}_k} = 1$ when $\gamma_{\mathrm{th}}^c \geq \frac{\beta_c}{\beta_1 + \beta_2}$ or $\gamma_{\mathrm{th}}^{p_k} \geq \frac{\beta_k}{\zeta\beta_c + \beta_j}$. When both conditions $\gamma_{\mathrm{th}}^c < \frac{\beta_c}{\beta_1 + \beta_2}$ and $\gamma_{\mathrm{th}}^{p_k} < \frac{\beta_k}{\zeta\beta_c + \beta_j}$ are satisfied, the probability expression in equation (10) can be represented as follows

$$\mathrm{OP}_{\mathrm{out}}^{\mathrm{D}_k} = \Pr\left\{ \mathcal{X}^2 < \max\left(\frac{\delta_{\mathrm{D}_k}^2 \gamma_{\mathrm{th}}^c}{P_{\mathrm{S}}(\beta_c - (\beta_1 + \beta_2)\gamma_{\mathrm{th}}^c)}, \frac{\delta_{\mathrm{D}_k}^2 \gamma_{\mathrm{th}}^{p_k}}{P_{\mathrm{S}}(\beta_k - (\zeta\beta_c + \beta_j)\gamma_{\mathrm{th}}^{p_k})} \right) \right\} \tag{11}$$

From (11), two cases can occur $\frac{\gamma_{\mathrm{th}}^c}{P_{\mathrm{S}}(\beta_c - (\beta_1 + \beta_2)\gamma_{\mathrm{th}}^c)} > \frac{\gamma_{\mathrm{th}}^{p_k}}{P_{\mathrm{S}}(\beta_k - (\zeta\beta_c + \beta_j)\gamma_{\mathrm{th}}^{p_k})}$ and $\frac{\gamma_{\mathrm{th}}^c}{P_{\mathrm{S}}(\beta_c - (\beta_1 + \beta_2)\gamma_{\mathrm{th}}^c)} \le \frac{\gamma_{\mathrm{th}}^{p_k}}{P_{\mathrm{S}}(\beta_k - (\zeta\beta_c + \beta_j)\gamma_{\mathrm{th}}^{p_k})}$.

In the case of $\frac{\gamma_{\mathrm{th}}^c}{P_{\mathrm{S}}(\beta_c - (\beta_1 + \beta_2)\gamma_{\mathrm{th}}^c)} > \frac{\gamma_{\mathrm{th}}^{p_k}}{P_{\mathrm{S}}(\beta_k - (\zeta\beta_c + \beta_j)\gamma_{\mathrm{th}}^{p_k})}$, we have $\frac{\gamma_{\mathrm{th}}^c}{\gamma_{\mathrm{th}}^{p_k}} + \gamma_{\mathrm{th}}^c > \frac{\beta_c}{\beta_k}(1 + \zeta\gamma_{\mathrm{th}}^c)$. The OP can be calculated as

$$\mathrm{OP}_{\mathrm{out}}^{\mathrm{D}_k} = \Pr\left\{ \mathcal{X}^2 < \frac{\delta_{\mathrm{D}_k}^2 \gamma_{\mathrm{th}}^c}{P_{\mathrm{S}}(\beta_c - (\beta_1 + \beta_2)\gamma_{\mathrm{th}}^c)} \right\} = F_{\mathcal{X}}\left(\sqrt{\frac{\delta_{\mathrm{D}_k}^2 \gamma_{\mathrm{th}}^c}{P_{\mathrm{S}}(\beta_c - (\beta_1 + \beta_2)\gamma_{\mathrm{th}}^c)}} \right) \tag{12}$$

Meanwhile $\frac{\gamma_{\mathrm{th}}^c}{P_{\mathrm{S}}(\beta_c - (\beta_1 + \beta_2)\gamma_{\mathrm{th}}^c)} \le \frac{\gamma_{\mathrm{th}}^{p_k}}{P_{\mathrm{S}}(\beta_k - (\zeta\beta_c + \beta_j)\gamma_{\mathrm{th}}^{p_k})}$, we have $\frac{\gamma_{\mathrm{th}}^c}{\gamma_{\mathrm{th}}^{p_k}} + \gamma_{\mathrm{th}}^c \le \frac{\beta_c}{\beta_k}(1 + \zeta\gamma_{\mathrm{th}}^c)$ and the OP is

$$\mathrm{OP}_{\mathrm{out}}^{\mathrm{D}_k} = \Pr\left\{ \mathcal{X}^2 < \frac{\delta_{\mathrm{D}_k}^2 \gamma_{\mathrm{th}}^{p_k}}{P_{\mathrm{S}}(\beta_k - (\zeta\beta_c + \beta_j)\gamma_{\mathrm{th}}^{p_k})} \right\} = F_{\mathcal{X}} \sqrt{\frac{\delta_{\mathrm{D}_k}^2 \gamma_{\mathrm{th}}^{p_k}}{P_{\mathrm{S}}(\beta_k - (\zeta\beta_c + \beta_j)\gamma_{\mathrm{th}}^{p_k})}} \tag{13}$$

To determine the CDF of $a_{\mathrm{SD}_k} + \sum_{i=1}^{N} a_{\mathrm{SR}_i} a_{\mathrm{R}_i\mathrm{D}_k} = \mathcal{X}$, moment functions can be employed as shown in [13]. The n^{th} moment of a_{SD_k} follows from (7) and (8) in [14]

$$\mu_{a_{\mathrm{SD}_k}}(n) = \mathbb{E}\left\{ a_{\mathrm{SD}_k}^n \right\} = \frac{\Gamma(m_{a_{\mathrm{SD}_k}} + \frac{n}{2})}{\Gamma(m_{a_{\mathrm{SD}_k}})} \left(\frac{m_{a_{\mathrm{SD}_k}}}{\Omega_{a_{\mathrm{SD}_k}}} \right)^{-\frac{n}{2}} \tag{14}$$

Thus, the specific moments of a_{SD_k} follow directly from equation (14)

$$\mu_{a_{\mathrm{SD}_k}}(1) = \frac{\Gamma(m_{a_{\mathrm{SD}_k}} + \frac{1}{2})}{\Gamma(m_{a_{\mathrm{SD}_k}})} \left(\sqrt{\frac{\Omega_{a_{\mathrm{SD}_k}}}{m_{a_{\mathrm{SD}_k}}}} \right) \text{ and } \mu_{a_{\mathrm{SD}_k}}(2) = \frac{\Gamma(m_{a_{\mathrm{SD}_k}} + 1)}{\Gamma(m_{a_{\mathrm{SD}_k}})} \left(\frac{\Omega_{a_{\mathrm{SD}_k}}}{m_{a_{\mathrm{SD}_k}}} \right) = \Omega_{a_{\mathrm{SD}_k}} \tag{15}$$

In addition, the PDF of $a_{\mathrm{SR}_i} a_{\mathrm{R}_i\mathrm{D}_k}$ is given by

$$f_{a_{\mathrm{SR}_i} a_{\mathrm{R}_i\mathrm{D}_k}}(v) = \int_0^{\infty} \frac{1}{u} f_{a_{\mathrm{R}_i\mathrm{D}_k}}\left(\frac{v}{u} \right) f_{a_{\mathrm{SR}_i}}(u) du \tag{16}$$

Substituting (8) into (16), we have

$$f_{a_{\mathrm{SR}_i}a_{\mathrm{R}_i\mathrm{D}_k}}(v)=\frac{4}{\Gamma(m_{a_{\mathrm{SR}_i}})\Gamma(m_{a_{\mathrm{R}_i\mathrm{D}_k}})}\left(\frac{m_{a_{\mathrm{SR}_i}}}{\Omega_{a_{\mathrm{SR}_i}}}\right)^{m_{a_{\mathrm{SR}_i}}}\left(\frac{m_{a_{\mathrm{R}_i\mathrm{D}_k}}}{\Omega_{a_{\mathrm{R}_i\mathrm{D}_k}}}\right)^{m_{a_{\mathrm{R}_i\mathrm{D}_k}}}v^{2m_{a_{\mathrm{R}_i\mathrm{D}_k}}-1}$$
$$\times\int_0^\infty u^{2m_{a_{\mathrm{SR}_i}}-2m_{a_{\mathrm{R}_i\mathrm{D}_k}}-1}\exp\left(-\frac{m_{a_{\mathrm{SR}_i}}u^2}{\Omega_{a_{\mathrm{SR}_i}}}-\frac{m_{a_{\mathrm{R}_i\mathrm{D}_k}}v^2}{\Omega_{a_{\mathrm{R}_i\mathrm{D}_k}}u^2}\right)du \tag{17}$$

Applying [15, Eq. (3.478.4)], the PDF in (17) can be written

$$f_{a_{\mathrm{SR}_i}a_{\mathrm{R}_i\mathrm{D}_k}}(v)=\frac{4\left(\frac{m_{a_{\mathrm{SR}_i}}m_{a_{\mathrm{R}_i\mathrm{D}_k}}}{\Omega_{a_{\mathrm{SR}_i}}\Omega_{a_{\mathrm{R}_i\mathrm{D}_k}}}\right)^{\frac{m_{a_{\mathrm{SR}_i}}+m_{a_{\mathrm{R}_i\mathrm{D}_k}}}{2}}}{\Gamma(m_{a_{\mathrm{SR}_i}})\Gamma(m_{a_{\mathrm{R}_i\mathrm{D}_k}})}v^{m_{a_{\mathrm{SR}_i}}+m_{a_{\mathrm{R}_i\mathrm{D}_k}}-1}\mathcal{K}_{m_{a_{\mathrm{SR}_i}}-m_{a_{\mathrm{R}_i\mathrm{D}_k}}}\left(2v\sqrt{\frac{m_{a_{\mathrm{SR}_i}}m_{a_{\mathrm{R}_i\mathrm{D}_k}}}{\Omega_{a_{\mathrm{SR}_i}}\Omega_{a_{\mathrm{R}_i\mathrm{D}_k}}}}\right) \tag{18}$$

Accordingly, the expression for the n^{th} moment of $a_{\mathrm{SR}_i}a_{\mathrm{R}_i\mathrm{D}_k}$ is

$$\mu_{a_{\mathrm{SR}_i}a_{\mathrm{R}_i\mathrm{D}_k}}(n)\triangleq\mathbb{E}\left\{(a_{\mathrm{SR}_i}a_{\mathrm{R}_i\mathrm{D}_k})^n\right\}=\int_0^\infty v^n f_{a_{\mathrm{SR}_i}a_{\mathrm{R}_i\mathrm{D}_k}}(v)dv \tag{19}$$

With (18) substituted into (19), and using [15, Eq. (6.561.16)], the result becomes

$$\mu_{a_{\mathrm{SR}_i}a_{\mathrm{R}_i\mathrm{D}_k}}(n)=\left(\frac{m_{a_{\mathrm{SR}_i}}m_{a_{\mathrm{R}_i\mathrm{D}_k}}}{\Omega_{a_{\mathrm{SR}_i}}\Omega_{a_{\mathrm{R}_i\mathrm{D}_k}}}\right)^{-\frac{n}{2}}\frac{\Gamma(m_{a_{\mathrm{SR}_i}}+\frac{n}{2})\Gamma(m_{a_{\mathrm{R}_i\mathrm{D}_k}}+\frac{n}{2})}{\Gamma(m_{a_{\mathrm{SR}_i}})\Gamma(m_{a_{\mathrm{R}_i\mathrm{D}_k}})} \tag{20}$$

Define $\Psi=\sum_{i=1}^{N}a_{\mathrm{SR}_i}a_{\mathrm{R}_i\mathrm{D}_k}$; the n^{th} moment of Ψ is then given by

$$\mu_\Psi(n)\triangleq\mathbb{E}\left\{\Psi^n\right\}\sum_{n_1=0}^{n}\sum_{n_2=0}^{n_1}\cdots\sum_{n_{N-1}=0}^{n_{N-2}}\binom{n}{n_1}\binom{n_1}{n_2}\cdots\binom{n_{N-2}}{n_{N-1}}$$
$$\times\mu_{a_{\mathrm{SR}_i}a_{\mathrm{R}_i\mathrm{D}_k}}(n-n_1)\mu_{a_{\mathrm{SR}_i}a_{\mathrm{R}_i\mathrm{D}_k}}(n_1-n_2)\ldots\mu_{a_{\mathrm{SR}_i}a_{\mathrm{R}_i\mathrm{D}_k}}(n_{N-1}) \tag{21}$$

where $\binom{x}{y}=\frac{x!}{y!(x-y)!}$.

According to [14], the specific moments of Ψ can be derived from equations (20) and (21)

$$\mu_\Psi(1)=\sum_{i=1}^{N}\mu_{a_{\mathrm{R}_i\mathrm{D}_k}}(1)\ \text{ and }\ \mu_\Psi(2)=\sum_{i=1}^{N}\mu_{a_{\mathrm{SR}_i}a_{\mathrm{R}_i\mathrm{D}_k}}(2)+2\sum_{i=1}^{N}\sum_{i`=i+1}^{N}\left[\mu_{a_{\mathrm{SR}_i}a_{\mathrm{R}_i\mathrm{D}_k}}(1)\right]^2 \tag{22}$$

Finally, the n^{th} moment of $\mathcal{X}$ can be formulated as

$$\mu_{\mathcal{X}}(n)\triangleq\mathbb{E}\left\{(\Psi+a_{\mathrm{SD}_k})^n\right\}=\mathbb{E}\left\{\sum_{w=0}^{n}\binom{n}{w}\Psi^w\left(a_{\mathrm{SD}_k}\right)^{n-w}\right\}=\sum_{w=0}^{n}\binom{n}{w}\mu_\Psi(w)\mu_{a_{\mathrm{SD}_k}}(n-w) \tag{23}$$

$$\mu_{\mathcal{X}}(1)=\mu_\Psi(1)+\mu_{a_{\mathrm{SD}_k}}(1)\ \text{ and }\ \mu_{\mathcal{X}}(2)=\mu_\Psi(2)+\mu_{a_{\mathrm{SD}_k}}(2)+2\mu_\Psi(1)\mu_{a_{\mathrm{SD}_k}}(1) \tag{24}$$

As shown in [14], the CDF of $\mathcal{X}$ is derived based on the moment expression

$$F_{\mathcal{X}}(y)=1-\frac{1}{\Gamma(\delta)}\gamma(\delta,\varepsilon y)\ \text{ where }\ \delta=\frac{\left[\mu_{\mathcal{X}}(1)\right]^2}{\mu_{\mathcal{X}}(2)-\left[\mu_{\mathcal{X}}(1)\right]^2}\ \text{ and }\ \varepsilon=\frac{\mu_{\mathcal{X}}(1)}{\mu_{\mathcal{X}}(2)-\left[\mu_{\mathcal{X}}(1)\right]^2} \tag{25}$$

By synthesizing the above cases, the final expression of the OP at D_k for the RIS-assisted RSMA system is presented in (26). The OP of the considered system is

$$\mathrm{OP}_{\mathrm{out}}^{\mathrm{D}_k}=\begin{cases}1-\dfrac{1}{\Gamma(\delta_1)}\gamma\left(\delta,\varepsilon\sqrt{\dfrac{\delta_{\mathrm{D}_k}^2\gamma_{\mathrm{th}}^c}{P_{\mathrm{S}}(\beta_c-(\beta_1+\beta_1)\gamma_{\mathrm{th}}^c)}}\right) & \text{when } \dfrac{\gamma_{\mathrm{th}}^c}{\gamma_{\mathrm{th}}^{p_k}}+\gamma_{\mathrm{th}}^c>\dfrac{\beta_c}{\beta_k}(1+\zeta\gamma_{\mathrm{th}}^c)\\ 1-\dfrac{1}{\Gamma(\delta)}\gamma\left(\delta,\varepsilon\sqrt{\dfrac{\delta_{\mathrm{D}_k}^2\gamma_{\mathrm{th}}^{p_k}}{P_{\mathrm{S}}(\beta_k-(\zeta\beta_c+\beta_j)\gamma_{\mathrm{th}}^{p_k})}}\right) & \text{when } \dfrac{\gamma_{\mathrm{th}}^c}{\gamma_{\mathrm{th}}^{p_k}}+\gamma_{\mathrm{th}}^c\le\dfrac{\beta_c}{\beta_k}(1+\zeta\gamma_{\mathrm{th}}^c)\\ 1 \text{ when } \gamma_{\mathrm{th}}^c\ge\dfrac{\beta_c}{\beta_1+\beta_2} \text{ or } \gamma_{\mathrm{th}}^{p_k}\ge\dfrac{\beta_k}{\zeta\beta_c+\beta_j}\end{cases} \tag{26}$$

2.3. System energy efficiency analysis

The OP measures the reliability of communication links, while system throughput indicates the overall data transmission capability. High throughput ensures efficient bandwidth utilization, supports multiuser access, and meets data-intensive demands. Thus, OP captures reliability, whereas throughput reflects spectral efficiency and resource utilization. Based on [16], the throughput of the D_k in the RIS-assisted RSMA system is expressed as follows

$$\mathcal{T}_{\mathrm{D}_k}=\begin{cases}R_c\left(1-\mathrm{OP}_{\mathrm{out}}^{\mathrm{D}_k}\right) & \text{when } \dfrac{\gamma_{\mathrm{th}}^c}{\gamma_{\mathrm{th}}^{p_k}}+\gamma_{\mathrm{th}}^c>\dfrac{\beta_c}{\beta_k}(1+\zeta\gamma_{\mathrm{th}}^c)\\ R_{p_k}\left(1-\mathrm{OP}_{\mathrm{out}}^{\mathrm{D}_k}\right) & \text{when } \dfrac{\gamma_{\mathrm{th}}^c}{\gamma_{\mathrm{th}}^{p_k}}+\gamma_{\mathrm{th}}^c\le\dfrac{\beta_c}{\beta_k}(1+\zeta\gamma_{\mathrm{th}}^c)\end{cases} \tag{27}$$

where $\mathcal{T}_{\mathrm{D}_k}$ denotes the throughput at the destination node D_k, and $\mathrm{OP}_{\mathrm{out}}^{\mathrm{D}_k}$ is computed according to (26). In addition, energy efficiency (EE) is a key metric in RIS-assisted RSMA systems and is mathematically expressed as follows [17]

$$\eta_{\mathrm{EE}}=\frac{\mathcal{B}\mathcal{T}_{\mathrm{D}_k}}{P_{\sum}}, \tag{28}$$

$$P_{\sum}=P_{\mathrm{S}}+NP_{\mathrm{S_N}}+P_{\mathrm{S}^*}+P_{\mathrm{D}_1}+P_{\mathrm{D}_2} \tag{29}$$

where $\mathcal{B}$ denotes the system bandwidth, $P_{\sum}$ represents the total power consumption of the system, while $P_{\mathrm{S}},NP_{\mathrm{S_N}},P_{\mathrm{S}^*},P_{\mathrm{D}_1},P_{\mathrm{D}_2}$ denote the circuit dissipation power at the source S, at the n^{th} reflecting element of the RIS, and at the destination nodes D_1 and D_2, respectively.

3. RESULTS AND DISCUSSION

This section focuses on evaluating the OP of the RIS-assisted RSMA system, while highlighting the impact of key factors such as the power allocation for the common stream, the number of RIS elements, carrier frequency, Nakagami-*m* fading parameter, and the imperfection level of SIC. The proposed scheme is benchmarked against a conventional RIS-assisted two-user NOMA system to compare performance. Unless otherwise stated in the figures, the simulation parameters are set as follows: the node locations are $(x_{\mathrm{S}},y_{\mathrm{S}})=(0,0)$, $(x_{\mathrm{D}_1},y_{\mathrm{D}_1})=(95,0)$, $(x_{\mathrm{D}_2},y_{\mathrm{D}_2})=(100,0)$ and $(x_{\mathrm{RIS}},y_{\mathrm{RIS}})=(65,0)$. 10^8 Monte Carlo trial, and the wireless channels

follow the Nakagami-m model with $m=3$. For the RSMA scheme, the power allocation coefficients are set to $\beta_c=0.8$ and $\beta_1=\beta_2=0.1$, $R_c=0.8$ bit/s/Hz and $R_c=R_{p_1}=R_{p_2}=0.2$ bit/s/Hz, $\beta_1^{\text{NOMA}}=0.45$, $\beta_2^{\text{NOMA}}=0.55$, $R_c^{\text{NOMA}}=1.0$ bit/s/Hz, $\zeta=0.01$. $\mathcal{B}=10$ MHz $P_{\text{S}_\text{N}}=5.01$ mW, $P_{\text{S}^*}=P_{\text{D}_1}=P_{\text{D}_2}=10$ mW.

Moreover, the system employs a channel model compliant with 5G/B5G recommendations, in which the path loss for node $\Omega_{\mathcal{N}}$ is computed using the standard reference model specified in [14]

$$\Omega_{\mathcal{N}}=\text{G}_{\text{tx}}-22.7-26\log(f_c)-36.7\log(d)+\text{G}_{\text{rx}} \tag{30}$$

where G_{tx}, G_{rx} denote the antenna gains at the transmitter and receiver, respectively; f_c is the carrier frequency $(2\le f_c\le 6\text{GHz})$; and d is the distance between the transmitter and receiver.

Figure 2 compares the OP of D_1 and D_2 under two multiple access schemes, RSMA and NOMA, both assisted by the RIS with $N=70$ elements. The results indicate that RSMA consistently outperforms NOMA across the entire range of P_{S}. Specifically, at $P_{\text{S}}=18$ dBm, the OP of D_1 RSMA drops to 7.2×10^{-4}, which is approximately 29.94 dB lower than that of D_1 under NOMA (i.e., 7.1×10^{-1}). Similarly, for D_2, RSMA achieves an OP of 8.5×10^{-3}, representing an improvement of more than 16.15 dB compared to the NOMA counterpart 3.5×10^{-1}. This performance gain is mainly attributed to the ability of RSMA to efficiently divide user messages and allocate transmit power. Moreover, the simulation results closely match the theoretical analysis, thereby confirming the accuracy of the proposed closed-form expressions.

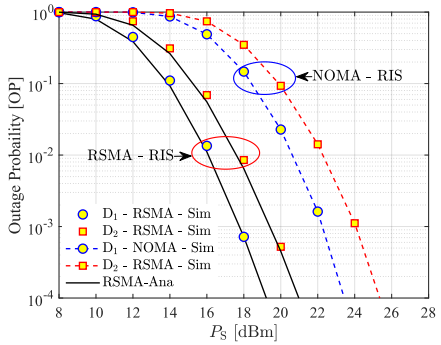

Figure 2. *Comparison of the OP between RIS-Assisted.*

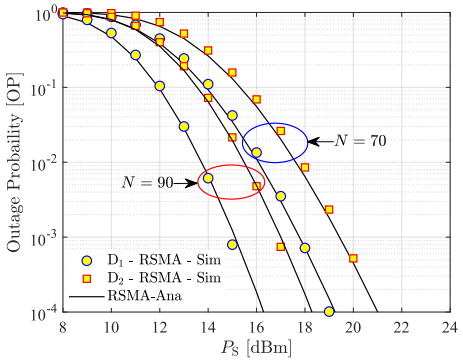

Figure 3. *OP versus parameter N.RSMA and RIS-Assisted NOMA systems.*

Figure 3 illustrates the OP of users D_1 and D_2 in the RIS-assisted RSMA system versus P_{S} while varying the RIS elements N. At a fixed P_{S}, increasing N from 70 to 90 significantly reduces the OP for both users. Specifically, at $P_{\text{S}}=16$ dBm, the OP of D_1 decreases from 1.6×10^{-2} to 2.8×10^{-3}, while that of D_2 drops from 8.2×10^{-2} to 1.0×10^{-2}. For example, we can observe at $P_{\text{S}}=22$ dBm, the OP of D_1 decreases marginally from 4×10^{-4} to 1.5×10^{-4}, and that of D_2 from 6.5×10^{-3} to 2.5×10^{-3}. These results suggest that although further performance gains are possible with increased P_{S} or N, the benefits diminish in high-power regimes.

Figure 4 shows how the OP varies with the imperfect SIC (ipSIC) factor ζ, highlighting its detrimental impact. However, increasing the number of RIS elements from $N=70$ to $N=75$ yields a substantial reduction in OP across the entire range of ζ. This result indicates that enlarging the RIS can effectively enhance system performance under ipSIC conditions.

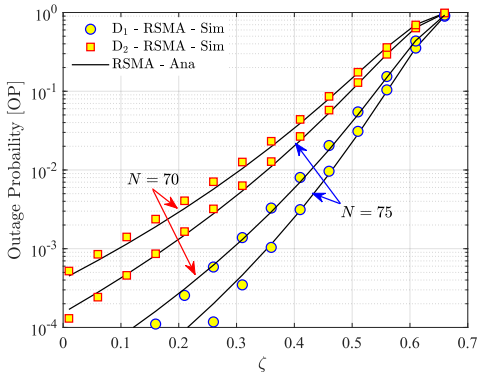

Figure 4. *OP versus parameter* ζ .

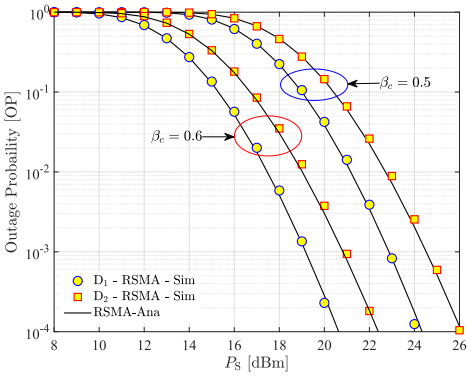

Figure 5. *OP versus parameter* β_c .

Figure 5 illustrates the OP of D_1 and D_2, in the RIS-assisted RSMA system, as a function of the transmit power P_S, with power allocation scenarios for the common stream, namely $\beta_c = 0.5$ and $\beta_c = 0.6$. Increasing β_c leads to a noticeable performance improvement at both D_1 and D_2, particularly in the low-power regime. Specifically, at $P_S = 18$ dBm, the OP of D_1 decreases from approximately 1.6×10^{-2} to 4.5×10^{-3}, while that of D_2 drops from 5×10^{-2} to around 6.5×10^{-3}. More power to the common stream enhances the decoding success probability at the weaker user during the SIC process, thereby improving the overall system reliability in the low SNR region. These results confirm the effectiveness of adaptive power allocation strategies in the design of RSMA systems.

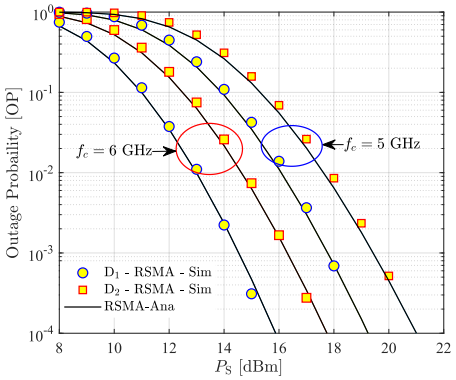

Figure 6. *OP versus parameter* f_c .

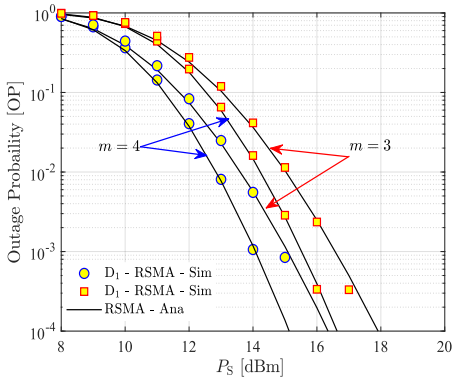

Figure 7. *OP versus parameter m.*

Figure 6 depicts the OP of D_1 and D_2 in the RIS-assisted RSMA system at two carrier frequencies, $f_c = 5$ GHz and $f_c = 6$ GHz. The results indicate a noticeable degradation in system performance as the carrier frequency increases. Specifically, at $f_c = 5$ GHz and $P_S = 14$ dBm, the OP values for D_1 and D_2 are 4.7×10^{-2} and 1.3×10^{-2}, respectively, while they increase to 1.4×10^{-1} and 3.9×10^{-2} at $f_c = 6$ GHz. These findings underscore the critical importance of selecting an appropriate carrier frequency in the design of RSMA systems, particularly under transmit power constraints. Favoring lower-frequency bands can be an effective strategy to mitigate path loss and enhance transmission reliability.

Figure 7 presents the OP of users D_1 and D_2, of the considered system. The results indicate that increasing the Nakagami-*m* parameter to $m = 3$ and $m = 4$ leads to a significant reduction in the OP across the entire transmit power range, reflecting a notable improvement in channel quality as the fading severity decreases.

Figure 8 with $N = 40$ and $m = 3$, the EE of RIS-assisted RSMA, and RIS-assisted NOMA is compared for $f_c = 2,4,6$ GHz. RIS-assisted RSMA consistently achieves higher EE: at $f_c = 2$ GHz, the peak reaches 12.1 bit/J at $P_S = -4$ dBm, whereas RIS-assisted NOMA attains only 10.8 bit/J at $P_S = 4$ dBm. As the frequency increases to 4 and 6 GHz, the peak EE of RIS-assisted RSMA decreases to 11.1 and 9.5 bit/J, respectively, due to higher path loss. In all cases, the maximum EE occurs at low-to-moderate transmit power ($P_S = 0$ to $P_S = 10$) before declining as capacity saturates while power consumption rises linearly.

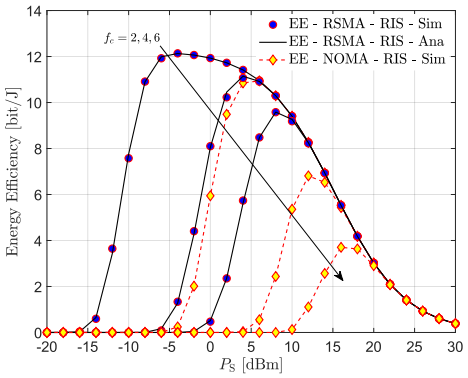

Figure 8. *EE of RSMA-RIS vs. NOMA-RIS.*

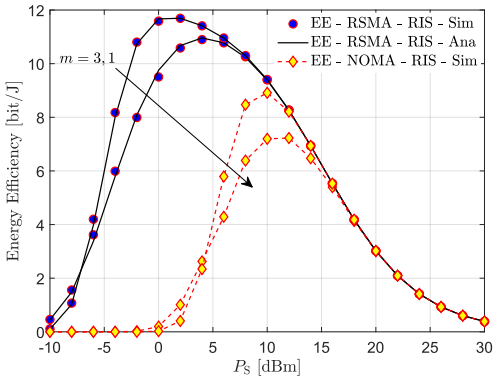

Figure 9. *EE of RSMA-RIS vs. NOMA-R under varying f_c under varying m.*

Figure 9 with $N = 40$ and $f_c = 3$ GHz, the effect of Nakagami - m fading is shown for $m = 1$ and $m = 3$. Under severe fading $m = 1$, RIS-assisted RSMA achieves about 10.9 bit/J at $P_S = 4$ dBm, while RIS-assisted NOMA yields 7.2 bit/J at $P_S = 10$ dBm. With improved fading $m = 3$, the peak EE of RIS-assisted RSMA rises to 11.7 bit/J, compared to only 8.9 bit/J for RIS-assisted NOMA. These findings confirm that RIS-assisted RSMA ensures superior EE and adapts more effectively to channel variations compared to RIS-assisted NOMA.

4. CONCLUSIONS

This paper proposes and analyzes RIS-assisted RSMA systems to enhance communication performance in wireless networks. Closed-form expressions for the OP and EE of two users are derived, considering the impact of ipSIC under Nakagami-m fading channels. Through theoretical analysis and extensive Monte Carlo simulations, the proposed system is shown to achieve superior performance, exhibiting significantly lower OP and higher EE compared to conventional RIS-assisted NOMA systems. Furthermore, a comprehensive analysis is conducted on the influence of key system parameters, such as the number of RIS elements, transmit power, carrier frequency, fading severity, and the level of SIC imperfection. Future research directions include extending the analysis to multi-user scenarios, optimizing RIS deployment strategies, and incorporating machine learning techniques to further improve the performance and adaptability of RIS-assisted RSMA systems in practical communication environments.

Acknowledgment: *This work is funded by Vietnam National Foundation for Science and Technology Development (NAFOSTED) under grant number 102.02-2023.11.*

REFERENCES

[1]. Liang, J., Chan, T.-T., and Pan, H. *"Minimizing age of collection for multiple access in wireless industrial Internet of Things"*, IEEE Internet of Things Journal, 11(2), 2753–2766, (2024).

[2]. Zhang, Y et al. *"Multiple access integrated adaptive finite blocklength for ultra-low delay in 6G wireless networks"*, IEEE Transactions on Wireless Communications, 23(3), 1670–1683, (2024).

[3]. Zheng, G., Wen, M., Wen, J., and Shan, C. *"Joint hybrid precoding and rate allocation for RSMA in*

near-field and far-field massive MIMO communications", IEEE Wireless Communications Letters, 13(4), 1034–1038, (2024).
[4]. Aswini, K. et al. *"Performance analyses of intelligent reflecting surface aided downlink multi-user rate-splitting multiple access system for 6G applications"*, Computer Networks, 242, 110271, (2024).
[5]. Huang, C., Zappone, A., Debbah, M., and Yuen, C. *"Achievable rate maximization by passive intelligent mirrors"*, in Proc. IEEE International Conference on Acoustics, Speech and Signal Processing (ICASSP), 3714–3718, (2018).
[6]. Huang, C., et al. *"Reconfigurable intelligent surfaces for energy efficiency in wireless communication"*, IEEE Transactions on Wireless Communications, 18(8), 4157–4170, (2019).
[7]. Yang, Z., et al. *"Energy efficient rate-splitting multiple access (RSMA) with reconfigurable intelligent surface"*, in IEEE International Conference on Communications Workshops, 1–6, (2020).
[8]. Z. Niu et al., *"Active RIS assisted rate-splitting multiple access network: Spectral and energy efficiency tradeoff,"* IEEE Wireless Commun. Lett., Vol. 12, No. 5, pp. 867–871, (2023).
[9]. Fang, T., et al. *"Fully connected reconfigurable intelligent surface aided rate-splitting multiple access for multi-user multi-antenna transmission"*, arXiv preprint arXiv:2201.07048, (2022).
[10]. Weinberger, K et al. *"Synergistic benefits in IRS- and RS-enabled C-RAN with energy-efficient clustering"*, IEEE Transactions on Wireless Communications, 1–1, (2022).
[11]. Bansal, A., Singh, K., and Li, C.-P. *"Analysis of hierarchical rate-splitting for intelligent reflecting surfaces-aided downlink multiuser MISO communications"*, IEEE Open Journal of the Communications Society, 2, 785–798, (2021).
[12]. Pham, X.-N., Nguyen, B.-C., Thi, T.-D., Nguyen, V.-V., Minh, B.-V., Kim, T., Nguyen, T.-N., and Le, A.-V. *"Enhancing data rate and energy efficiency of NOMA systems using reconfigurable intelligent surfaces for millimeter-wave communications"*, Digital Signal Processing, 151, 104553, (2024).
[13]. Do, T.-N., Kaddoum, G., Nguyen, T.-L., Da Costa, D.-B., and Haas, Z. J. *"Multi-RIS-aided wireless systems: Statistical characterization and performance analysis"*, IEEE Transactions on Communications, 69(12), 8641–8658, (2021).
[14]. Van, Q.-N., Nguyen, B.-C., Hoang, T.-M., Nguyen, H.-M., Nguyen, V.-V., Luu, G.-T., et al. *"Multiple RISs for enhancing the secrecy performance of NOMA systems over realistic Nakagami-m fading channels"*, IEEE Transactions on Vehicular Technology, 73(5), 6584–6599, (2023).
[15]. Jeffrey, A., and Zwillinger, D. *"Table of integrals, series, and products"*, Academic Press, (1994).
[16]. Singh, S.-K., Agrawal, K., Singh, K., and Li, C.-P. *"Outage probability and throughput analysis of UAV-assisted rate-splitting multiple access"*, IEEE Wireless Communications Letters, 10(11), 2528–2532, (2021).

TÓM TẮT

Phân tích xác suất dừng của hệ thống RSMA được hỗ trợ bởi RIS trên kênh fading Nakagami-*m*

Trong nghiên cứu này, chúng tôi đề xuất và phân tích một hệ thống RSMA có hỗ trợ bởi RIS. Khung nghiên cứu được thiết kế nhằm nâng cao hiệu quả truyền dẫn bằng cách khai thác đồng thời cả liên kết trực tiếp và liên kết phản xạ qua RIS để phục vụ hai người dùng. Xét đến tính thực tiễn, chúng tôi đưa vào mô hình sự không hoàn hảo của quá trình khử giao thoa liên tiếp (SIC). Dưới mô hình kênh fading Nakagami-m, các biểu thức dạng đóng cho xác suất dừng (OP) và hiệu quả năng lượng (EE) được dẫn xuất và kiểm chứng thông qua mô phỏng Monte Carlo với số vòng lặp lớn. Bên cạnh đó, một phân tích so sánh toàn diện với hệ thống NOMA có hỗ trợ bởi RIS cũng được thực hiện. Kết quả mô phỏng cho thấy hệ thống đề xuất vượt trội đáng kể so với NOMA về chỉ số OP. Các tác động của những tham số hệ thống chính, bao gồm số phần tử phản xạ RIS, công suất phát, tần số sóng mang, mức độ nghiêm trọng của fading và độ không hoàn hảo của SIC, đều được khảo sát chi tiết. Các kết quả đạt được cho thấy RSMA có hỗ trợ RIS là một giải pháp đầy hứa hẹn nhằm nâng cao độ tin cậy cho các mạng không dây 6G trong tương lai.

Từ khoá: Xác suất dừng; Hiệu quả năng lượng; Đa truy nhập phân chia theo tỷ lệ; Bề mặt thông minh tái cấu hình; Khử nhiễu liên tiếp không hoàn hảo.